



Article

Regional Assessment of Soil Moisture Active Passive Enhanced L3 Soil Moisture Product and Its Application in Agriculture

Liming Zhu ^{1,2}, Guizhi Tian ¹, Huifeng Wu ¹, Maohua Ding ^{1,*}, A-Xing Zhu ^{3,4,5,6} and Tianwu Ma ^{3,4,5}

¹ College of Hydraulic Science and Engineering, Yangzhou University, Yangzhou 225009, China; zhuliming@yzu.edu.cn (L.Z.)

² Foundation of Anhui Province Key Laboratory of Physical Geographic Environment, Chuzhou 239099, China

³ School of Geography, Nanjing Normal University, Nanjing 210023, China; tianwuma@nnu.edu.cn (T.M.)

⁴ Key Laboratory of Virtual Geographic Environment, Nanjing Normal University, Ministry of Education, Nanjing 210046, China

⁵ Jiangsu Center for Collaborative Innovation in Geographical Information Resource Development and Application, Nanjing 210046, China

⁶ Department of Geography, University of Wisconsin-Madison, Madison, WI 53706, USA

* Correspondence: 006997@yzu.edu.cn; Tel.: +86-18052097081

Abstract: Soil moisture (SM) is a crucial environmental variable, and it plays an important role in energy and water cycles. SM data retrieval based on microwave satellite remote sensing has garnered significant attention due to its spatial continuity, wide observational coverage, and relatively low cost. Validating the accuracy of satellite remote sensing SM products is a critical step in enhancing data credibility, which plays a vital role in ensuring the effective application of satellite remote sensing data across various fields. Firstly, this study focused on Henan Province and evaluated the accuracy of the SMAP Enhanced L3 Radiometer Global and Polar Grid Daily 9 km EASE-Grid Soil Moisture (SPL3SMP_E) product along with its application in agriculture. The evaluation was based on in situ SM data from 55 stations in Henan Province. The assessment metrics used in this study include mean difference (MD), root mean square error (RMSE), unbiased root mean square error (ubRMSE), and the Pearson correlation coefficient (R). The time span of this study is from 2017 to 2020. The evaluation results indicated that the SPL3SMP_E soil moisture product performs well, as reflected by an ubRMSE value of 0.045 (m^3/m^3), which was relatively close to the product's design accuracy of 0.04 (m^3/m^3). Moreover, the accuracy of the product was unaffected by temporal factors, but the product exhibited strong spatial aggregation, which was closely related to land use types. Then, this study explored the response of the SPL3SMP_E product to irrigation signals. The precipitation and irrigation data from Henan Province were employed to investigate the response of the SPL3SMP_E soil moisture product to irrigation. Our findings revealed that the SPL3SMP_E soil moisture product was capable of capturing over 70% of irrigation events in the study area, indicating its high sensitivity to irrigation signals in this region. In this study, the SPL3SMP_E product was also employed for monitoring agricultural drought in Henan Province. The findings revealed that the collaborative use of the SPL3SMP_E soil moisture product and machine learning algorithms proves highly effective in monitoring significant drought events. Furthermore, the integration of multiple indices demonstrated a notable enhancement in the accuracy of drought monitoring. Such an evaluation holds significant implications for the effective application of satellite remote sensing SM data in agriculture and other domains.

Keywords: satellite-based soil moisture products; L-band; SMAP; irrigation signal



Citation: Zhu, L.; Tian, G.; Wu, H.; Ding, M.; Zhu, A.-X.; Ma, T. Regional Assessment of Soil Moisture Active Passive Enhanced L3 Soil Moisture Product and Its Application in Agriculture. *Remote Sens.* **2024**, *16*, 1225. <https://doi.org/10.3390/rs16071225>

Academic Editors: John Kalogiros, Jianzhong Lu and Marios Anagnostou

Received: 20 February 2024

Revised: 18 March 2024

Accepted: 26 March 2024

Published: 30 March 2024



Copyright: © 2024 by the authors. Licensee MDPI, Basel, Switzerland. This article is an open access article distributed under the terms and conditions of the Creative Commons Attribution (CC BY) license (<https://creativecommons.org/licenses/by/4.0/>).

1. Introduction

Soil moisture is a crucial component of the Earth's ecosystems, playing a significant role in the interactions among water bodies, land, and the atmosphere [1]. Soil moisture has been designated as one of the 50 essential climate variables by the Global Climate

Observing System [2]. Soil moisture data have been extensively employed in various research fields, such as climate change studies, drought monitoring, and terrestrial carbon cycling [3–5].

In situ soil moisture observations and retrievals via satellite remote sensing data are two ways to obtain surface soil moisture data [6]. In situ soil moisture observations can provide the most direct reflection of soil water at various depths, but this method suffers from the issue of the sparse distribution of monitoring stations [7]. Satellite remote sensing retrieval has emerged as the most effective means for soil moisture observation due to its advantages of spatial continuity, wide observation coverage, and cost-effectiveness. Previous studies have extensively explored satellite remote sensing retrieval of soil moisture, capitalizing on these advantages [8,9]. For example, Li et al. [10] summarized the key issues in the satellite remote sensing retrieval of soil moisture and provided an outlook on its future development trends. Satellite remote sensing retrieval can be categorized into optical remote sensing and microwave remote sensing. Compared to optical remote sensing, microwave remote sensing offers several advantages, including less susceptibility to atmospheric interference, deeper sensing capabilities, and a more direct physical relationship between remote sensing information and soil moisture [11]. Specifically, passive microwave remote sensing stands out for its significant advantages, such as wide coverage, short repeat cycles, and high sensitivity to soil moisture variations. Consequently, it has emerged as the most promising approach for soil moisture retrieval [12].

In recent years, significant progress has been made in the utilization of satellite remote sensing technology for soil moisture retrieval, leading to the more expedited and effective acquisition of regional-scale soil moisture data. Various institutions have successively released soil moisture products based on microwave satellite remote sensing data. For example, the European Space Agency (ESA) developed the Soil Moisture and Ocean Salinity (SMOS) mission (2009–present) [13], the National Aeronautics and Space Administration (NASA) offered the Soil Moisture Active Passive (SMAP) mission (2015–present) [14], and the European Organization for the Exploitation of Meteorological Satellites (EUMETSAT) provided the Advanced Scatterometer (ASCAT) mission (2007–present) [15]. These products use passive microwave remote sensing data detected in various bands, enabling their synergistic application on a global scale. The main bands include the X-band [16], C-band [17], P-band [18], and L-band [19]. The L-band is considered the optimal frequency range for the remote sensing of soil moisture due to its strong penetration capability [20]. SMOS and SMAP are the two newest soil moisture products retrieved based on L-band satellite remote sensing data.

The validation and assessment of satellite remote sensing soil moisture products are essential to ensure data accuracy before applying them. A large number of previous studies have conducted research on the accuracy of SMOS and SMAP data [21,22]. For example, Fernandez-Moran et al. [23] conducted a validation of the SMOS-IC product, revealing that it exhibits high correlation and low unbiased root mean square error (ubRMSE) in the majority of pixels. Similarly, Chan et al. [24] validated the accuracy of the SMAP level 2 passive soil moisture product (L2_SM_P) at a spatial resolution of 36 km. Through a comparison of in situ data and satellite data using multiple indicators, they found that the data's ubRMSE closely approached the product's mission requirement of 0.04 (cm³/cm³). Moreover, Zhang et al. [25] evaluated the global spatiotemporal accuracy characteristics of SMAP satellite soil moisture based on international ground-based soil moisture observations. The results indicated a high level of accuracy for the SMAP satellite soil moisture product. Zhu et al. [26] compared soil moisture data from 131 stations in the upstream region of the Huaihe River with satellite soil moisture data. The research findings indicated that the accuracy of the SMAP soil moisture product in that region is higher than that of the SMOS product. Similarly, Kim et al. [27] analyzed the strengths and weaknesses of two L-band soil moisture products across different climate zones and land cover types on a global scale. The results revealed that the SMAP product outperformed SMOS in terms of accuracy on approximately 69% of the Earth's surface. Li et al. [28] evaluated the perfor-

mance of the SMAP SM product and SMAP Enhanced SM product in the Tibetan Plateau. The results indicated that the SMAP product showed stronger correlation (0.64–0.88) and the enhanced product provided finer details at the regional scale.

In the application of those soil moisture products, previous studies have leveraged soil moisture products derived from microwave satellite remote sensing to extract irrigation parameters, recognizing the intrinsic link between agricultural irrigation and variations in soil moisture. Several studies have explored the feasibility of detecting irrigation signals using remote sensing soil moisture data [29–34]. Zhu et al. [30] established an irrigation signal recognition model using microwave satellite remote sensing soil moisture to extract irrigation information. By identifying irrigation signals from satellite soil moisture data, they successfully extracted irrigation information. Hao et al. applied a 5-points moving average method to eliminate errors caused by the low resolution of SMAP data. Then they detected irrigation signals in the southern part of Hebei Province, China, based on multiple data sources, including SMAP data, MODIS data, and meteorological data. The overall accuracy of irrigation signal detection reached 77%. Jacopo et al. [32] proposed a dual-scale analysis to study the detectability of irrigation occurrences in central Italy using satellite soil moisture. The results indicated a 60% overlap between satellite-detected irrigation signals and actual irrigation events. Furthermore, Pascal et al. [34] compared the response of SMAP and SMOS in detecting irrigation signals in Southern India at a resolution of 25 km. They found that SMAP exhibited a stronger response to irrigation signals and then estimated the irrigation water use for the rainy and dry seasons. In addition, soil moisture derived from microwave satellite remote sensing soil moisture products can be directly applied to agricultural drought monitoring [4,35]. For example, Iliana E et al. [35] assessed the accuracy of assimilating soil moisture retrievals from the Soil Moisture Active Passive (SMAP) mission into the USDA-FAS Palmer model for agricultural drought monitoring. The results showed that the SMAP satellite soil moisture product combined with Palmer soil moisture estimates (PM) can be very effective in monitoring agricultural drought. Cao et al. [4] evaluated the accuracy and performance of two satellite soil moisture products, Soil Moisture and Ocean Salinity (SMOS) and Soil Moisture Active Passive (SMAP), in drought monitoring assessment between 2015 and 2018 in the North China Plain. The study pointed out that SMAP outperformed SMOS in SM data validation and drought monitoring in the North China Plain region.

These studies highlight the importance of satellite soil moisture products for agricultural production and provide valuable references for their application in agriculture. Employing remote sensing soil moisture data to extract irrigation parameters and drought monitoring can aid in optimizing irrigation management, enhancing agricultural water resource utilization efficiency, and providing decision support for crop growth and yield. However, there is a scarcity of research in the Henan region concerning the validation of satellite soil moisture product accuracy and the application performance of the satellite soil moisture product. Several questions concerning this research area remain unaddressed: (1) What are the disparities between the L-band SMAP satellite soil moisture product and in situ soil moisture measurements in the Henan region? (2) What is the accuracy and spatial distribution of the SPL3SMP_E soil moisture product in this area? (3) How does the SPL3SMP_E soil moisture product perform in the agriculture applications? Our objective is to address these questions and provide valuable insights for enhancing the retrieval algorithm of the SPL3SMP_E soil moisture product. To achieve this goal, we plan to employ on-site measurements from 55 meteorological stations in Henan province for the assessment of the SMAP satellite L-band product. Our specific objectives are as follows: (1) To assess the accuracy of the SPL3SMP_E soil moisture product in the study area and investigate its correlation with environmental factors and (2) to explore the application of the SPL3SMP_E soil moisture product in agriculture, including irrigation signal detection and agriculture drought monitoring. By achieving the aforementioned objectives, we hope to provide more accurate data for satellite soil moisture monitoring in the region and

offer reliable decision-making support for areas such as agricultural irrigation and water resource management.

2. Study Area

This study focused on Henan province in China as the study area, with a total area of 167,000 km². The terrain in the region exhibits higher elevations in the west and lower elevations in the east, with predominantly flat plains. The northern, western, and southern boundaries are characterized by a semi-circular distribution of mountainous areas along the provincial border (Figure 1a).

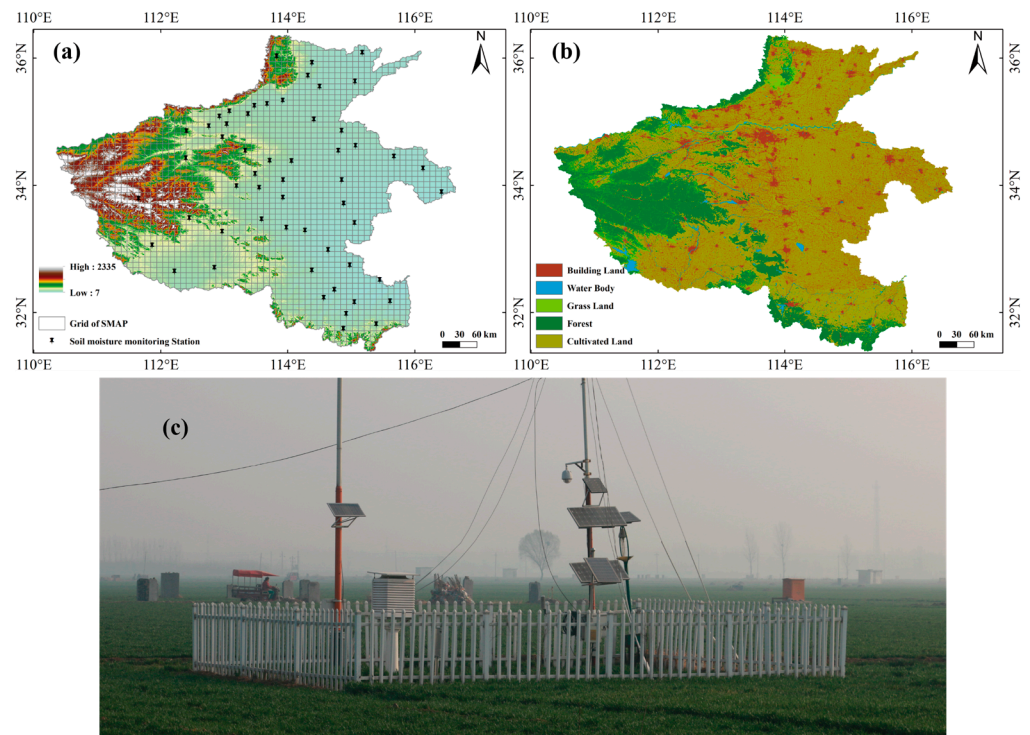


Figure 1. (a) Elevation of the study area, SMAP grid, and distribution of 55 monitoring stations; (b) land use of the study area; (c) in situ soil moisture monitoring stations and its surrounding environment.

As shown in Figure 1, the primary land use type in the research area is cultivated farmland, with wheat cultivation covering 54% of the total grain sowing area. Additionally, there are areas dedicated to corn, potatoes, and other crops. Forests and grass lands cover approximately 24.53% of the land, primarily concentrated in the mountainous regions. The majority of the study area is located in the warm-temperate zone, with the southern part crossing into the subtropical zone. It falls under a continental monsoon climate, transitioning from the northern subtropical zone to the warm-temperate zone. The average annual temperature stands at 15.8 °C. The average annual precipitation measures 594.3 mm, with the bulk of the rainfall occurring between June and August. There are a total of 110 in situ sites in the study area. In order to ensure the quality of the satellite SM, the pixels were filtered by the summed fraction of urban, wetland, and open water. Finally, a total of 55 soil moisture monitoring stations were chosen in the region (Figure 1c). To ensure data completeness, we ultimately selected soil moisture data from the 55 stations.

3. Datasets and Methods

3.1. Datasets

3.1.1. In Situ Soil Moisture Dataset

In situ soil moisture data were obtained from 55 soil water monitoring stations within the study area, as shown in Figure 1a. These in situ soil moisture monitoring stations are

primarily situated in the plain area and are thus unaffected by topographical variations. During the data collection process, a time domain reflectometry (TDR) sensor was employed to probe soil moisture at regular intervals of 10 cm starting from the surface, providing data that cover a depth range of 1 m below the ground surface. The error of the TDR sensor is $\pm 3\%$. The in situ soil moisture data from these monitoring stations were provided by the Agricultural Meteorological Station of Henan Province Meteorological Bureau, which were collected at six o'clock am (Beijing time) every day from 1 January 2017 to 1 January 2021. Peng et al. [36] suggested that soil moisture data obtained at a depth of 10 cm from the monitoring stations exhibit the closest correspondence to satellite-derived soil moisture. Therefore, in this validation experiment, in situ soil moisture data collected at a depth of 10 cm from the monitoring stations were used as the reference.

3.1.2. SMAP Enhanced Level 3 (L3) Product

The concept of the SMAP mission [14] involves employing radar backscatter and radiometer measurements to achieve soil moisture retrieval with a spatial resolution of up to 3 km [37]. The L-band radiometer component of the SMAP mission, which operates at a center frequency of 1.4 GHz, is placed in a near-polar sun-synchronous orbit. Its primary mission objective is to provide daily global observations of soil moisture at depths ranging from 0 to 5 cm, with observations acquired consistently at 6 a.m. UTC [24]. However, due to a radar malfunction in July 2015, there has been a lack of high-resolution soil moisture information [38]. To obtain high-resolution data, we adopted the level 3 spatially enhanced soil moisture product (L3_SM_P_E 005). This level 3 product is a daily global composite of level 2 geophysical retrievals for the entire UTC day. It is derived from the Backus–Gilbert interpolation of radiometer brightness temperature measurements and is posted on a grid with a resolution of 9 km. The product represents volumetric water content at a depth of 5 cm below the ground surface [39,40]. The daily SMAP SM data retrievals from morning overpasses were chosen, and the data were filtrated according to the retrieval_qual_flag_am.

3.1.3. Auxiliary Datasets

The proportion of Land Use and Land Cover Change (LUCC) is derived from the GlobeLand30 dataset, which is a global land cover dataset developed in China with a spatial resolution of 30 m. The update of this dataset was initiated by the Ministry of Natural Resources in 2014, and the latest version, GlobeLand30 2020, has been successfully updated (<https://www.webmap.cn/mapDataAction.do?method=globalLandCover>) (accessed on 3 May 2023). The 1 km \times 1 km resolution elevation data (dataset of 1 km resolution DEM in China, 2020) used in this study can be downloaded from the website of the Institute of Geographic Sciences and Natural Resources Research, Chinese Academy of Sciences (<https://www.resdc.cn/Default.aspx>) (accessed on 20 May 2023).

The daily precipitation data and irrigation data we used were sourced from the Agricultural Meteorological Station of Henan Province Meteorological Bureau. The irrigation method employed at the monitoring stations is fixed quota irrigation.

In this study, different scales of vegetation indices were obtained using the Google Earth Engine (GEE) cloud platform [41]. The image data adopted in this paper include the normalized difference vegetation index (NDVI) product MOD13A1, evapotranspiration (ET) product MOD16A2, and land surface temperature (LST) product MOD11A1, and the time-fixed number of years are 2017~2020. Specifically, image data with a resolution of 9 km and a temporal interval of 16 days between 2017 and 2020 were extracted from GEE. The relevant data can be accessed from the website (<https://earthengine.google.com/>) (accessed on 25 May 2023).

3.2. Methods

3.2.1. Statistical Analysis Methods for the Performance of the SPL3SMP_E Product

Four statistical indicators are used in this study to assess the accuracy of the satellite-based soil moisture product, namely, MD, RMSE, ubRMSE, and R [42,43]. The formulas for these four statistical indicators are presented in Table 1. In Table 1, S_{SM} denotes the soil moisture values obtained from the SMAP satellite, and M_{SM} denotes the in situ soil moisture measurements from the monitoring stations, both expressed in (cm^3/cm^3). When calculating R, μ_S denotes the mean of satellite-derived soil moisture; μ_M denotes the mean of in situ soil moisture measurements, both expressed in (cm^3/cm^3); δ_S denotes the standard deviation of satellite-derived soil moisture; and δ_M denotes the standard deviation of in situ soil moisture measurements, both expressed in (cm^3/cm^3).

Table 1. Statistical metrics used for soil moisture evaluation.

Metric	Symbol	Definition	Range	Perfect Score
Mean Difference	MD	$\frac{\sum_{i=1}^N (S_{SM_i} - M_{SM_i})}{N}$	$[-\infty, +\infty]$	0
Root Mean Square Error	RMSE	$\sqrt{\frac{\sum_{i=1}^N (S_{SM_i} - M_{SM_i})^2}{N}}$	$[0, +\infty]$	0
Unbiased Root Mean Square Error	ubRMSE	$\sqrt{(RMSE)^2 - (MD)^2}$	$[0, +\infty]$	0
Pearson Correlation Coefficient	R	$\frac{\sum_{i=1}^N (S_{SM_i} - \mu_S)(M_{SM_i} - \mu_M)}{(N-1)\delta_S\delta_M}$	$[-1, 1]$	1

3.2.2. Temporal and Spatial Correlation Analysis

The one-way ANOVA test was employed to examine the significant variations in the time series of the four statistical indicators. At the 95% confidence level, the data for each indicator over four years were divided into two subsets: the first half of the year and the second half of the year. Consequently, each statistical indicator had four treatment groups, each comprising two replicates. By employing the LSD and Waller–Duncan methods for mean difference analysis and assessing the significance p -value, we aim to determine whether noteworthy distinctions among the various treatment groups exist.

Moran's index was employed to quantify the spatial auto-correlation of four statistical indicators. With values ranging between -1 and 1, this index quantifies the level of spatial association in the data. Positive values signify spatial positive correlation, negative values indicate spatial negative correlation, and a value of zero suggests spatial randomness in the data. The Z-score represents how many standard deviations a data point deviates from the mean, reflecting the confidence level. A higher Z-score (positive value) or lower Z-score (negative value) indicates a higher confidence level. When the Z-score is greater than 1.96 or less than -1.96, the confidence level is typically at 95%. If the Z-score is greater than 2.58 or less than -2.58, the confidence level is generally at 99%. The research process involves two main steps: global Moran's index analysis and local Moran's index analysis, which includes clustering and outlier analysis.

3.2.3. Irrigation Signal Detection of the SPL3SMP_E Product

The assimilation of surface observation data is a method that relies solely on high-precision satellite soil moisture data to detect irrigation signals. The method identifies the irrigation signal based on precipitation greater than 5 mm during the increasing period of soil moisture. When there is no precipitation greater than 5 mm during the increasing period of soil moisture, and the increased soil moisture is greater than $0.04 \text{ m}^3/\text{m}^3$, then the increase in soil moisture is considered to be caused by irrigation. Conversely, the increase in soil moisture is considered to be caused by precipitation. A similar method has been used in previous studies [44,45].

In this study, we adopted this approach to verify irrigation signals in the study area. Figure 2 displays the line graph illustrating both in situ soil moisture and satellite soil moisture throughout the entire growth period of winter wheat in the study area, along with the corresponding bar chart representing precipitation amounts. The in situ soil moisture and satellite soil moisture exhibited consistent trends. Notably, at the four time points marked in the chart, there was relatively low precipitation. However, both in situ and satellite soil moisture showed an increase. After consulting the agricultural meteorological data from local weather stations, agricultural irrigation was confirmed to have taken place during these four instances. Therefore, it can be inferred that the satellite soil moisture product is capable of capturing irrigation signals. In summary, this study validated the presence of the irrigation signal in the study area by observing the phenomenon of no rainfall or insufficient rainfall leading to an increase in soil moisture over a period of time; meanwhile, satellite soil moisture increased abnormally.

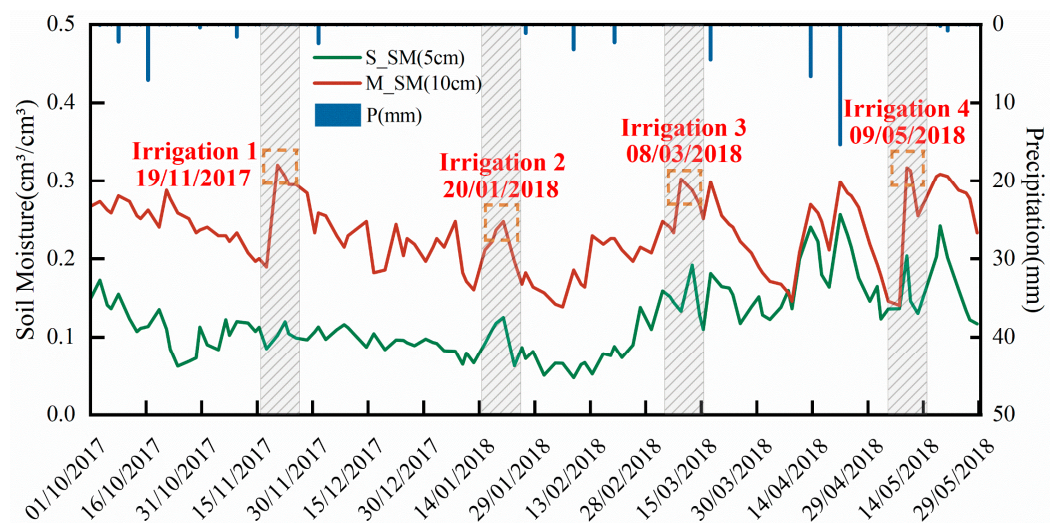


Figure 2. The response of the SPL3SMP_E product to irrigation during the 2018 winter wheat growing season.

3.2.4. Drought Monitoring of Winter Wheat with the SPL3SMP_E Product

Developing agricultural drought monitoring models involves the Random Forest (RF) and Multi-layer Perceptron (MLP) algorithms, respectively. Among these, the independent variables of the training sample set consist of SPL3SMP_E soil moisture product data along with other remote sensing indices [46,47], while the dependent variable is the classification of drought levels based on soil moisture content at a depth of 20 cm in situ [48], and its classification is shown in Table 2.

Table 2. Drought classification of relative soil moisture.

Grade	Type	Relative Soil Moisture at Depth of 20 cm
1	No drought	$60\% < RSM$
2	Mild drought	$50\% < RSM \leq 60\%$
3	Moderate drought	$40\% < RSM \leq 50\%$
4	Severe drought	$30\% < RSM \leq 40\%$
5	Extreme drought	$RSM \leq 30\%$

RF is a machine learning algorithm based on ensemble learning. The core concept is to employ the Bootstrap resampling technique to repeatedly and randomly draw samples with replacement from the original training set, thereby generating a new set of training set. Subsequently, multiple decision trees are constructed by using these bootstrapped datasets. Employing a voting mechanism, the final result is determined by the predictions from these multiple decision trees.

MLP is a type of feed-forward artificial neural network consisting of 3 to 5 layers of neurons, including an input layer, an output layer, and several hidden layers, all of which are fully connected. The MLP algorithm can be employed for both regression and classification tasks. During training, a supervised back-propagation learning method is typically utilized to obtain the values of various parameters within the network.

In April, during the jointing and heading stage of winter wheat, the water requirement is at its peak, making it the most susceptible period to drought throughout the entire growth cycle. In this study, an 80% random sample from the dataset is chosen as the training set, with the remaining 20% allocated for the testing set, to construct the two aforementioned machine learning models. Subsequently, SPL3SMP_E soil moisture product data and other remote sensing datasets for the study area on April 6, 2018, are selected to conduct comprehensive drought monitoring across the region. Additionally, spatial auto-correlation analysis is performed on the results of drought monitoring.

4. Results

4.1. Overall Accuracy of the SPL3SMP_E Soil Moisture Product

An analysis of the overall accuracy of the SPL3SMP_E soil moisture product is presented for the period from 2017 to 2020, while ensuring that the satellite grid and ground stations correspond spatially. Furthermore, its performance is evaluated on a monthly scale. The evaluation metrics for the SPL3SMP_E soil moisture product are presented in Table 3, and the performance of these evaluation metrics on a monthly scale are illustrated in Figure 3. Through an analysis of the metrics in Table 3, a comprehensive assessment of the accuracy of the SPL3SMP_E soil moisture product can be derived. Meanwhile, Figure 3 provides a more intuitive representation of how these evaluation metrics vary over time. It should be pointed out that a total of 130 pairs of SM data in each year were used to calculate the metrics in Table 3.

Table 3. Evaluation metrics for the SPL3SMP_E soil moisture product.

Year	Symbol	MD (m ³ /m ³)	RMSE (m ³ /m ³)	ubRMSE (m ³ /m ³)	R
	2017	−0.08	0.13	0.05	0.42
	2018	−0.07	0.13	0.05	0.38
	2019	−0.06	0.12	0.04	0.28
	2020	−0.07	0.12	0.04	0.44
	Overall accuracy	−0.07	0.125	0.045	0.38

Table 3 reveals notable consistency in the results of the indicators across each year. Notably, MD consistently displays negative values, while ubRMSE consistently achieves minimal values. Only R shows a relatively substantial change in 2019. In this study area, the ubRMSE of the SMAP soil moisture product is approximately 0.04 (m³/m³). This outcome indicates that the evaluation accuracy of the SPL3SMP_E soil moisture product aligns closely with its intended design accuracy. This finding is consistent with conclusions drawn from research conducted in other regions [49–51]. Simultaneously, the consistently negative values of MD may indicate a prevalent underestimation of soil moisture by the SPL3SMP_E soil moisture product in this specific region. Additionally, the significant variation observed in R during 2019 may necessitate further research and explanation.

As shown in Figure 3, it becomes evident that different statistical indicators reflect temporal discrepancies in the accuracy of the satellite soil moisture product. For the MD, the product accuracy reaches its highest value in July and its lowest value in January, exhibiting an overall trend of lower precision at the beginning and end of the year, with higher precision during the mid-year period. As for RMSE, the product accuracy peaks in September, but the overall trend shows higher precision in the first half of the year compared to the second half. Conversely, ubRMSE, which combines MD and RMSE, exhibits the opposite trend to MD, with higher product accuracy at the beginning and end of the year

and lower accuracy during the middle of the year. However, all indicators remain below 0.1 (m^3/m^3), almost approaching 0, thus rendering them suitable for verifying the accuracy of a satellite product for each month. Furthermore, by comparing the monthly R values over the four-year span while excluding outliers, it is evident that R consistently remains greater than 0. This result indicates a positive correlation between the soil moisture data from the in situ and the SPL3SMP_E soil moisture data. Moreover, there are no apparent consistent trends in R over the time scale, suggesting that R exhibits randomness over time.

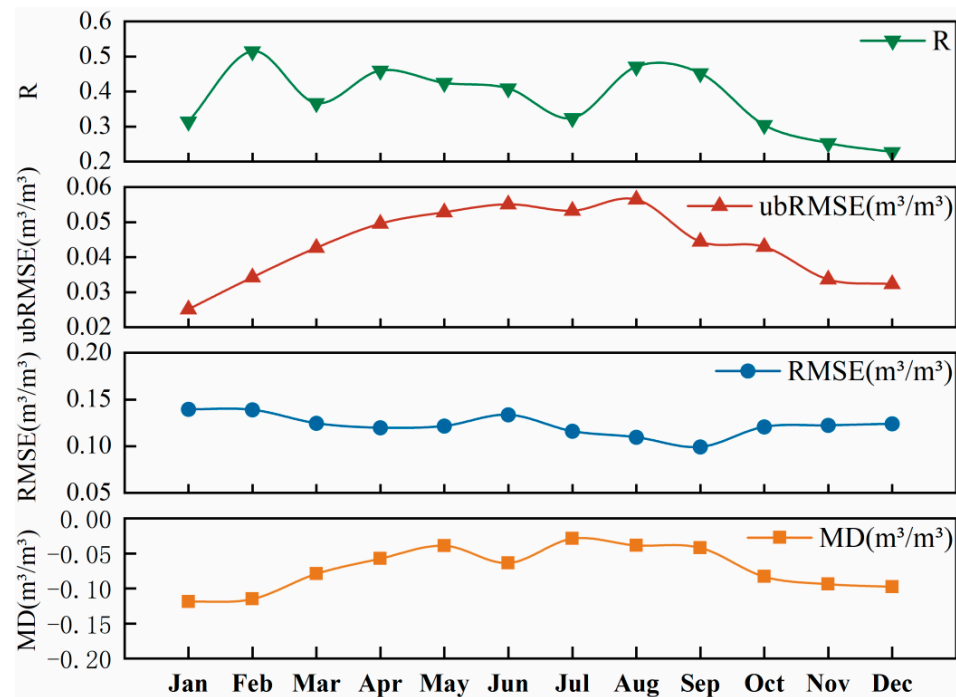


Figure 3. Monthly variations in accuracy metrics for the SPL3SMP_E soil moisture product.

To investigate the presence of randomness in the statistical indicator results, we employed one-way ANOVA (analysis of variance) to perform a statistical analysis on several metrics on a monthly scale. The results of the one-way ANOVA test are presented in Table 4. Table 4 presents an analysis of the temporal significance differences among the four statistical indicators. Notably, all p -values are significantly greater than 0.05, indicating no statistically significant differences among the various statistical indicators over time.

Table 4. One-way ANOVA for variability in SPL3SMP_E soil moisture product accuracy metrics.

Symbol	K (Degree of Freedom)	F	P
MD	7	0.50	0.70
RMSE	7	0.43	0.75
ubRMSE	7	0.72	0.59
R	7	2.77	0.18

Figure 4 displays a comparison of the variance between the first half and second half of each year for the four indicators. The results indicate that “a” is not significant, implying that the variance of data within each group of data is consistent, and statistically significant differences in data are not observed. In other words, the overall accuracy of the satellite product does not exhibit variation over time. Based on the combined results from Table 4 and Figure 4, we conclude that no significant differences over time are shown by the four statistical indicators in this study. Additionally, the overall accuracy of the satellite soil moisture product remains stable over the long-term time scale.

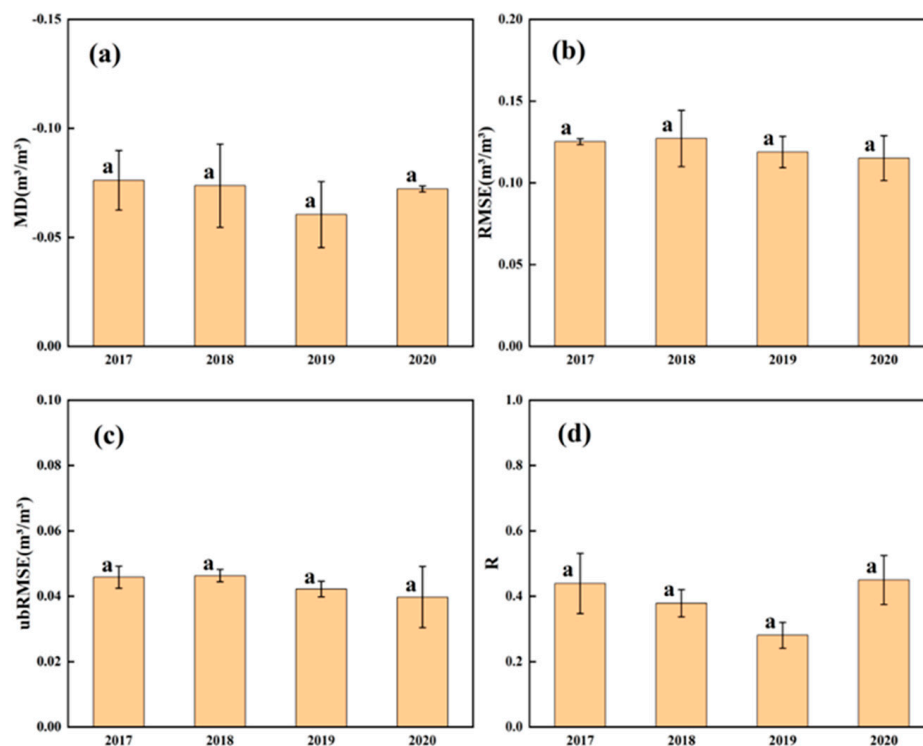


Figure 4. Significant differences in SPL3SMP_E soil moisture product accuracy over time: (a) MD; (b) RMSE; (c) ubRMSE; (d) R.

4.2. Spatial Distribution of the Accuracy Indicators

Through data preprocessing, we only use data with one-to-one correspondence between grids and ground stations. Therefore, we used the Kriging interpolation method to spatially analyse the accuracy metrics for the whole study area. Kriging interpolation is a method for optimal linear, unbiased interpolation estimation of spatially distributed data. The method not only takes into account the spatial correlation between known data points, but also provides information on the variance of the estimated accuracy. Figure 5 provides a visual representation of the spatial distribution of the MD indicator at the site, while Figure 6 presents the spatial distribution of the RMSE indicator. Figure 7 displays the spatial distribution of the ubRMSE indicator, and Figure 8 exhibits the spatial distribution of the R indicator. These interpolation images serve to offer a more intuitive insight into the spatial distribution of the soil moisture statistical indicators within the study area.

In Figure 5, the interpolated map of the MD indicator reveals that values in the eastern and northeastern regions are comparatively lower, while values in the southeastern region are higher. The central and western areas have values closer to 0, covering a substantial portion of the total area. This phenomenon provides strong evidence supporting the high accuracy of the satellite soil moisture product. The difference in RMSE shown in Figure 6 exhibits a similar trend as MD, with an increasing proportion of areas exhibiting values close to 0 over time. It further confirms the high accuracy of the satellite soil moisture product. Figure 7, illustrating the interpolated map of ubRMSE, demonstrates an increasing trend in spatial distribution from the central or northwestern regions toward the eastern region. However, it is essential to note that the absolute values of this indicator are relatively small. Despite the observed variation trend, it effectively underscores the product's high accuracy. In Figure 8, R shows a consistent increasing trend from the northwest to the southeast over the four-year period. After removing several outliers, all R values are positive, indicating a positive correlation between satellite soil moisture and in situ soil moisture.

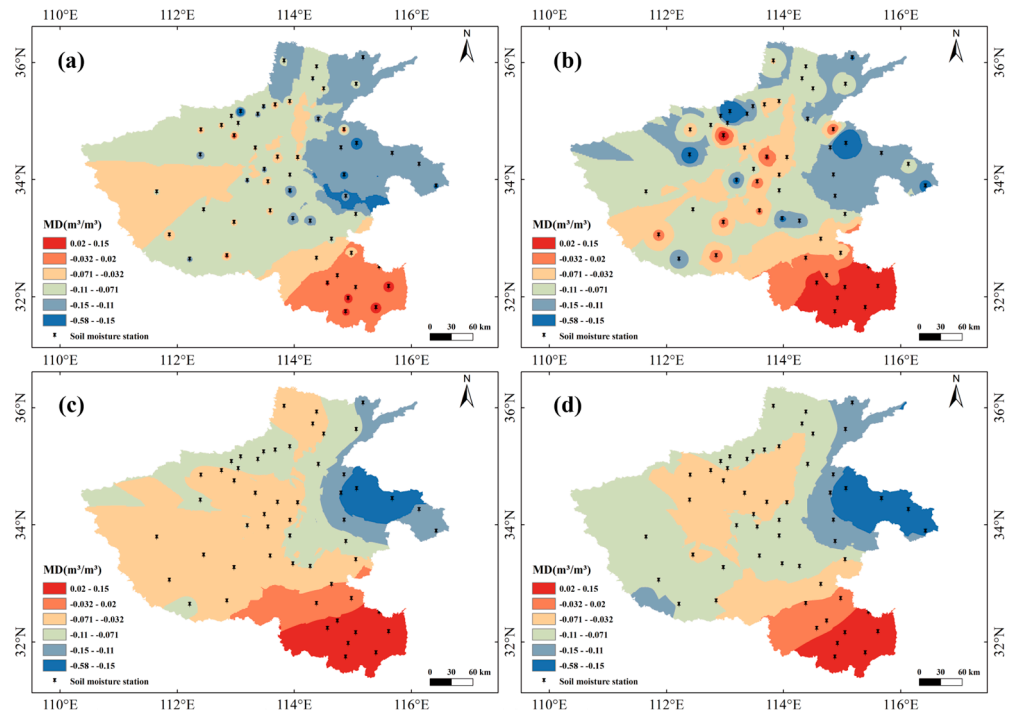


Figure 5. Spatial distribution of MD metrics for the SPL3SMP_E product, interpolated from the average annual MD at the site: (a) 2017; (b) 2018; (c) 2019; (d) 2020.

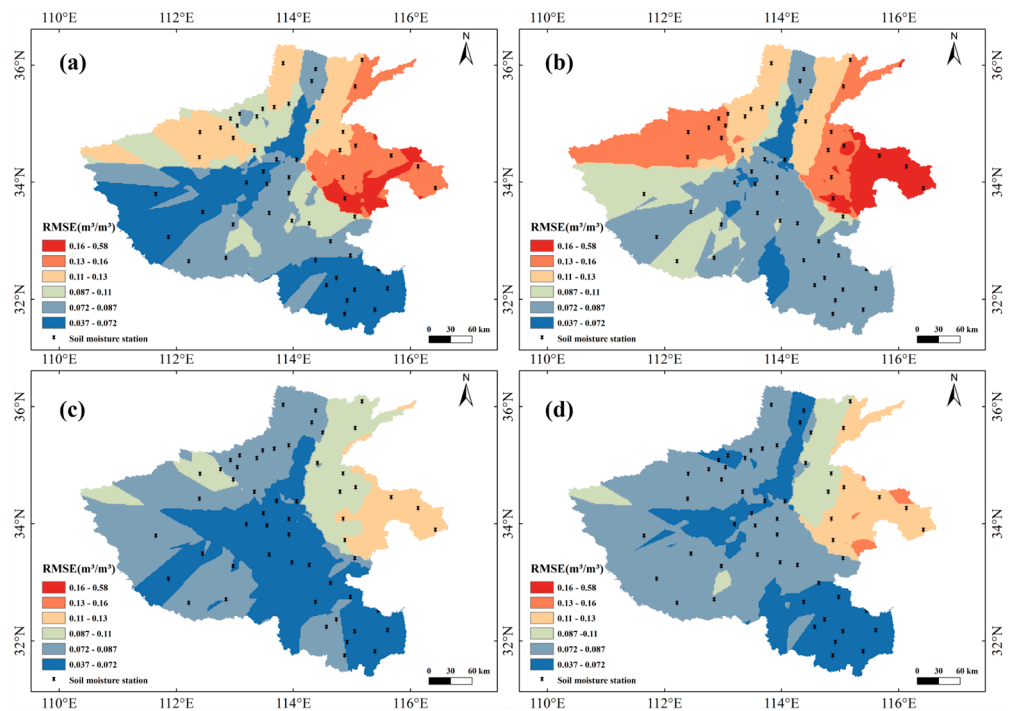


Figure 6. Spatial distribution of RMSE metrics for the SPL3SMP_E product, interpolated from the average annual RMSE at the site: (a) 2017; (b) 2018; (c) 2019; (d) 2020.

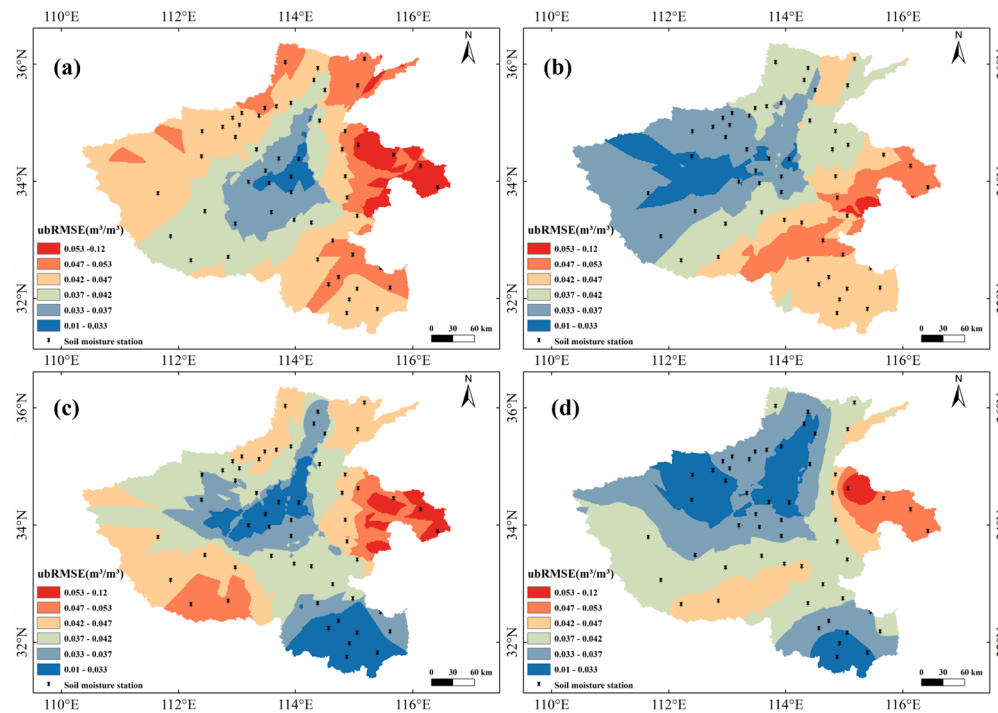


Figure 7. Spatial distribution of ubRMSE metrics for SPL3SMP_E product, interpolated from the average annual ubRMSE at the site: (a) 2017; (b) 2018; (c) 2019; (d) 2020.

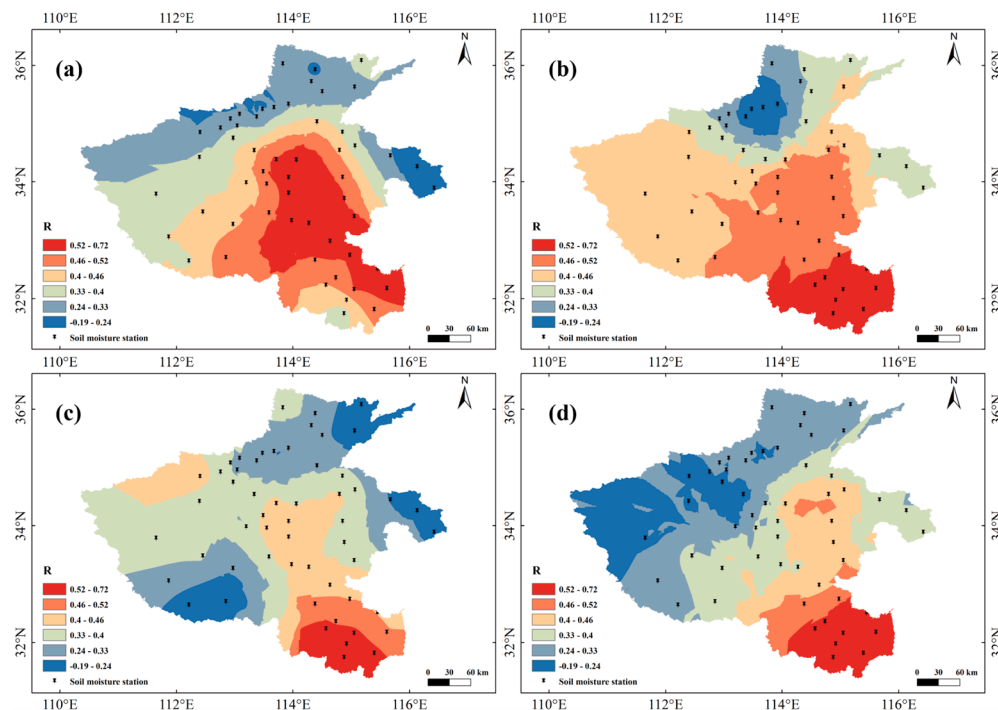


Figure 8. Spatial distribution of R metrics for SPL3SMP_E product, interpolated from the average annual R at the site: (a) 2017; (b) 2018; (c) 2019; (d) 2020.

4.3. Spatial Aggregation Features of the Accuracy Indicators

To investigate the aggregation features of the accuracy indicators of the SPL3SMP_E soil moisture product, this study calculated the Moran's index of the four accuracy indicators. Table 5 provides a summary of the Moran's index and their corresponding Z-scores. Table 5 shows that all Moran's index values for the indicators are close to or greater than 0, and their corresponding Z-scores all exceed 1.96. These findings indicate that all four

indicators exhibit significant spatial clustering and have a high level of confidence, generally exceeding 95%. Taking MD as an example, Figure 9 displays the spatial clustering distribution of the indicator within the study area. Approximately 70% of grid cells exhibit significant spatial clustering, indicating no significant differences in spatiality. Outliers are primarily concentrated in the southernmost region of the study area, demonstrating a high-value clustering characteristic. In summary, the statistical indicators exhibit no significant temporal variation but demonstrate spatial clustering patterns across the study area.

Table 5. Moran's index and Z-scores for the four accuracy indicators for the SPL3SMP_E product.

		MD	RMSE	ubRMSE	R
2017	Moran's-I	0.17	0.05	0.10	0.36
	Z-score	2.82	2.27	2.00	4.08
2018	Moran's-I	0.22	0.04	0.03	0.26
	Z-score	2.64	2.33	3.68	2.99
2019	Moran's-I	0.30	0.07	0.07	0.42
	Z-score	3.57	4.16	2.18	4.72
2020	Moran's-I	0.33	0.12	0.01	0.32
	Z-score	3.91	1.99	2.40	3.66

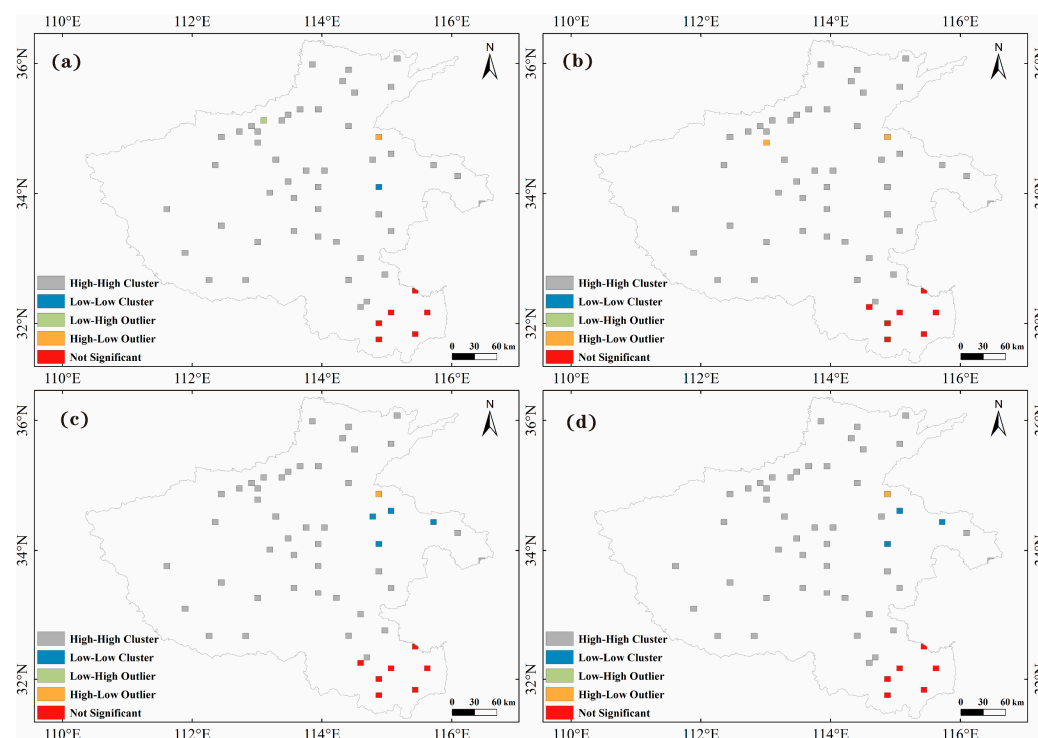


Figure 9. Local spatial auto-correlation of accuracy indicators for the SPL3SMP_E product: (a) 2017; (b) 2018; (c) 2019; (d) 2020.

4.4. Response of Satellite Soil Moisture Product to Irrigation

The accurate capture of irrigation signals is of significant importance for agricultural production management and decision making. Based on in situ soil moisture data and precipitation data, we evaluated the detection capability of the SPL3SMP_E soil moisture product for irrigation signals. Table 6 shows an in-depth study of the capture capability of the SPL3SMP_E satellite soil moisture product for the winter wheat growing season irrigation signals at the 53990 (Hebi City) site from 2017 to 2020. We assessed the irrigation signal capture capability of the satellite product in different months, as shown in Table 6.

Table 6. Response of SPL3SMP_E soil moisture product to irrigation signals at site 53990.

Irrigation Time	SM the Day before (cm ³ /cm ³)	SM on the Day (cm ³ /cm ³)	SM the Day after (cm ³ /cm ³)	The Satellite Captures or Not (Y/N)
	P the Day before (mm)	P on the Day (mm)	P the Day after (mm)	
5 March 2017	0.19 0	0.35 0	0.34 0	Y
1 May 2017	0.17 0	0.36 0	0.36 0	Y
19 November 2017	0.17 0	0.19 0	0.22 0	Y
20 January 2018	0.24 0	0.23 0	0.29 0	Y
8 March 2018	0.24 0	0.23 0	0.31 0	Y
9 May 2018	0.14 0	0.12 0	0.32 0	Y
25 October 2018	0.15 0	0.15 0.50	0.32 0	Y
24 January 2019	0.28 0.10	0.26 0	0.25 0	N
30 March 2019	0.15 0	0.15 0	0.33 0	Y
19 May 2019	0.16 0	0.15 0	0.32 0	Y
21 March 2020	0.19 0	0.19 0	0.34 0	Y
20 April 2020	0.24 0.80	0.22 0	0.20 0	N
19 May 2020	0.20 0	0.18 0	0.17 0	N
8 June 2020	0.10 0	0.10 0	0.32 0	Y
25 October 2020	0.17 0	0.17 0	0.32 0	Y

As noted in Table 6, the SPL3SMP_E soil moisture product exhibited strong capability in capturing irrigation signals, with over 70% of irrigation events being detected by the satellite over the four-year period. This conclusion was further validated using data from other stations, which confirmed that the satellite SPL3SMP_E soil moisture product captured irrigation signals reliably and fairly accurate. However, it is worth noting that these signals were often reflected in the data on the day after irrigation due to a delay of 12–24 h, which is described in the official documentation (<https://smap.jpl.nasa.gov/observatory/operations/>) (accessed on 16 March 2023). The success rate of regional irrigation capture was higher than that of site-specific irrigation due to the current low resolution of the satellite soil moisture products. Although this validation experiment uses a resolution of 9 km, there were still multiple agricultural activities within a grid cell, making it difficult to precisely target irrigation at a specific site. Furthermore, various factors, including the climate, crops, and soil, led to the soil moisture remaining unchanged or decreasing after irrigation, which was a normal occurrence [52]. This occurrence also contributed to the satellites' inability to accurately capture irrigation signals. In conclusion, it is essential to consider factors such as data latency and resolution when using them, although the satellite soil moisture product demonstrated strong capabilities in capturing irrigation signals.

4.5. Drought Monitoring with the SPL3SMP_E Product

Training the Random Forest (RF) and Multi-layer Perceptron (MLP) models involves utilizing 80% of the datasets for the training process, while the remaining 20% is reserved

for validation. The results indicate that the RF model achieves an accuracy of 83% when solely relying on satellite soil moisture data for agricultural drought monitoring. When incorporating both satellite soil moisture and other remote sensing indices, the accuracy of the RF model increases to 92%. Similarly, the MLP model achieves an accuracy of 78% when solely utilizing satellite soil moisture data for agricultural drought monitoring, which rises to 94% when integrating satellite soil moisture with other remote sensing indices. Hence, there is no significant difference in the accuracy of agricultural drought monitoring between the two models. However, the combined use of satellite soil moisture and other remote sensing indices (NDVI, LET, ET) yields higher accuracy in agricultural drought monitoring compared to solely relying on SPL3SMP_E soil moisture data.

Figure 10a illustrates the agricultural drought distribution solely considering satellite soil moisture monitoring using the RF algorithm. Figure 10b depicts the agricultural drought distribution considering both satellite soil moisture and other remote sensing indices monitoring using the RF algorithm. Figure 10 c,d, respectively, present the agricultural drought distribution monitored in the study area using the MLP algorithm. From the monitoring results, it is evident that the eastern region of the study area has experienced relatively severe drought events, while extensive no-drought areas are observed in the south. In the RF algorithm, the monitoring results based on a single factor show significant dispersion. However, in multi-factor monitoring, drought is predominantly concentrated in the eastern and western regions. The MLP algorithm demonstrates the highest accuracy in multi-factor drought monitoring. However, it exhibits lower sensitivity to drought events in single-factor monitoring, which may be attributed to the suitability of the algorithm itself.

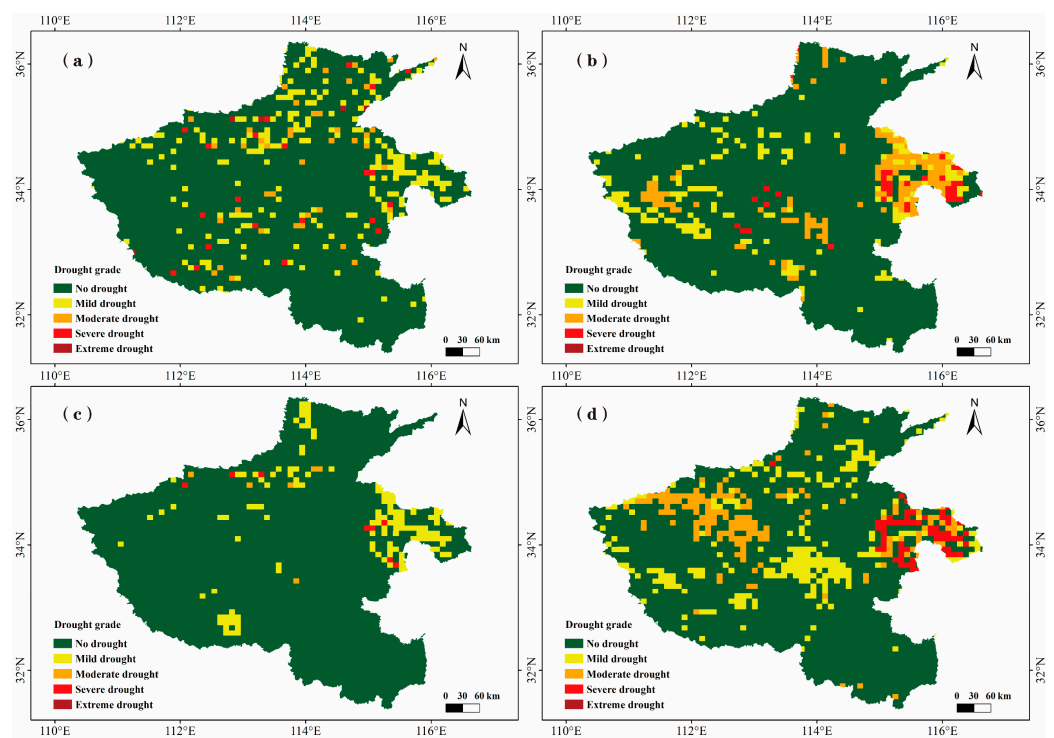


Figure 10. Henan Province drought distribution map (4 June 2018): (a) RF single-factor monitoring; (b) RF multi-factor monitoring; (c) MLP single-factor monitoring; (d) MLP multi-factor monitoring.

Figure 11 illustrates the spatial clustering of drought events under four different drought monitoring approaches. The clustering results indicate a pronounced high-high clustering phenomenon in the eastern part of the study area, where the frequency of agricultural drought events is significantly higher than in surrounding areas, with a significance level of 99%. This finding is substantiated by reference to the Agricultural Meteorological Monthly Report of Henan Province, which documented a notably severe drought event in the eastern part of the study area in early April 2018.

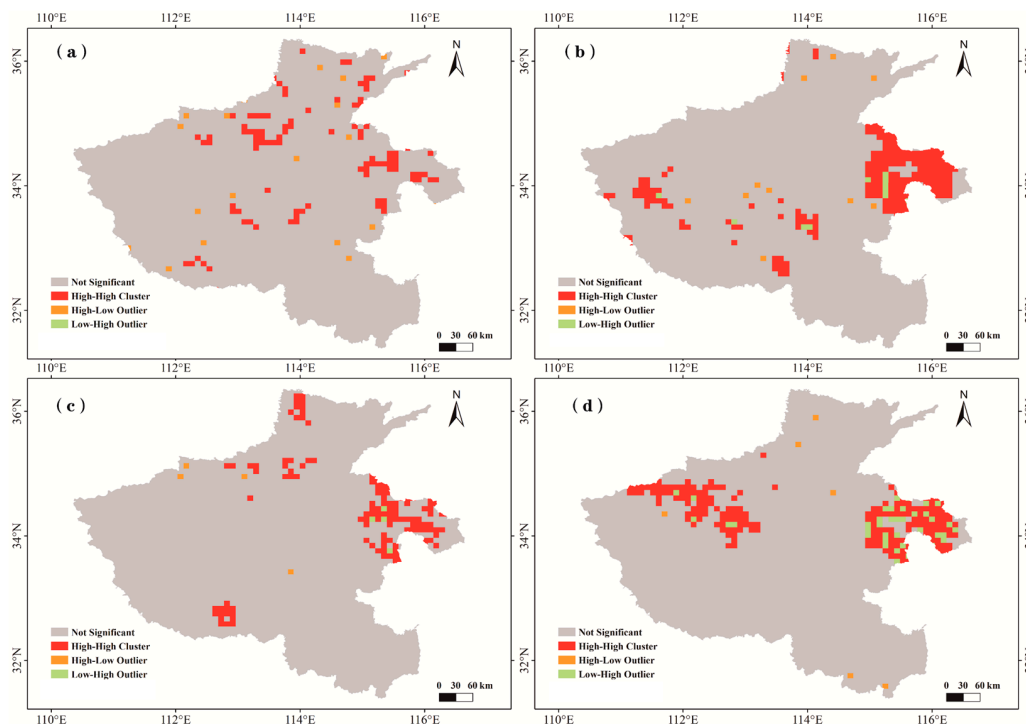


Figure 11. Local spatial auto-correlation of agricultural drought in Henan Province (4 June 2018): (a) RF single-factor monitoring; (b) RF multi-factor monitoring; (c) MLP single-factor monitoring; (d) MLP multi-factor monitoring.

In conclusion, the SPL3SMP_E satellite soil moisture product can be effectively utilized for agricultural drought monitoring, demonstrating its capability to capture major drought events. Further integration of additional remote sensing indices with soil moisture data contributes to enhancing the accuracy of drought monitoring. This integrated approach proves to be effective in monitoring drought events that may be challenging to observe using individual factors alone.

5. Discussion

The accuracy of the SPL3SMP_E soil moisture product appears to be unaffected by temporal factors but exhibits a strong spatial clustering pattern. Therefore, this study further explored the relationship between the accuracy of the satellite soil moisture product and environmental factors, including the land use proportion and vegetation indices. The land use was classified into five categories: cultivated land, forest, grass land, water bodies, and building land. The normalized difference vegetation index (NDVI) was selected as the vegetation index. Table 7 provides an overview of the MD, R, and correlation coefficients of these six factors. Through the computation of these correlation coefficients, we can gain insights into the extent of the relationship between the SPL3SMP_E soil moisture product and different land use types and vegetation indices.

Table 7. Correlation between the accuracy indexes (MD and R) and environmental factors.

	Proportion of Cultivated	Proportion of Forest	Proportion of Grass	Proportion of Water	Proportion of Building	NDVI
MD	0.47	−0.16	−0.10	−0.27	0.48	−0.22
R	0.32	−0.05	−0.18	0.01	0.35	0.15

Concerning MD, the indicators positively correlate with the proportion of cultivated land and building land, while they negatively correlate with the proportion of forests, grass lands, and NDVI. Regarding R, the indicators positively correlate with the proportion of

cultivated land, water bodies, building land, and NDVI, and they negatively correlate with the proportion of forests and grass lands. The MD's scatter plot and linear regression concerning the proportion of the five land use types and average NDVI are shown in Figure 12. R's scatter plot and linear regression concerning the proportion of the five land use types and average NDVI are shown in Figure 13.

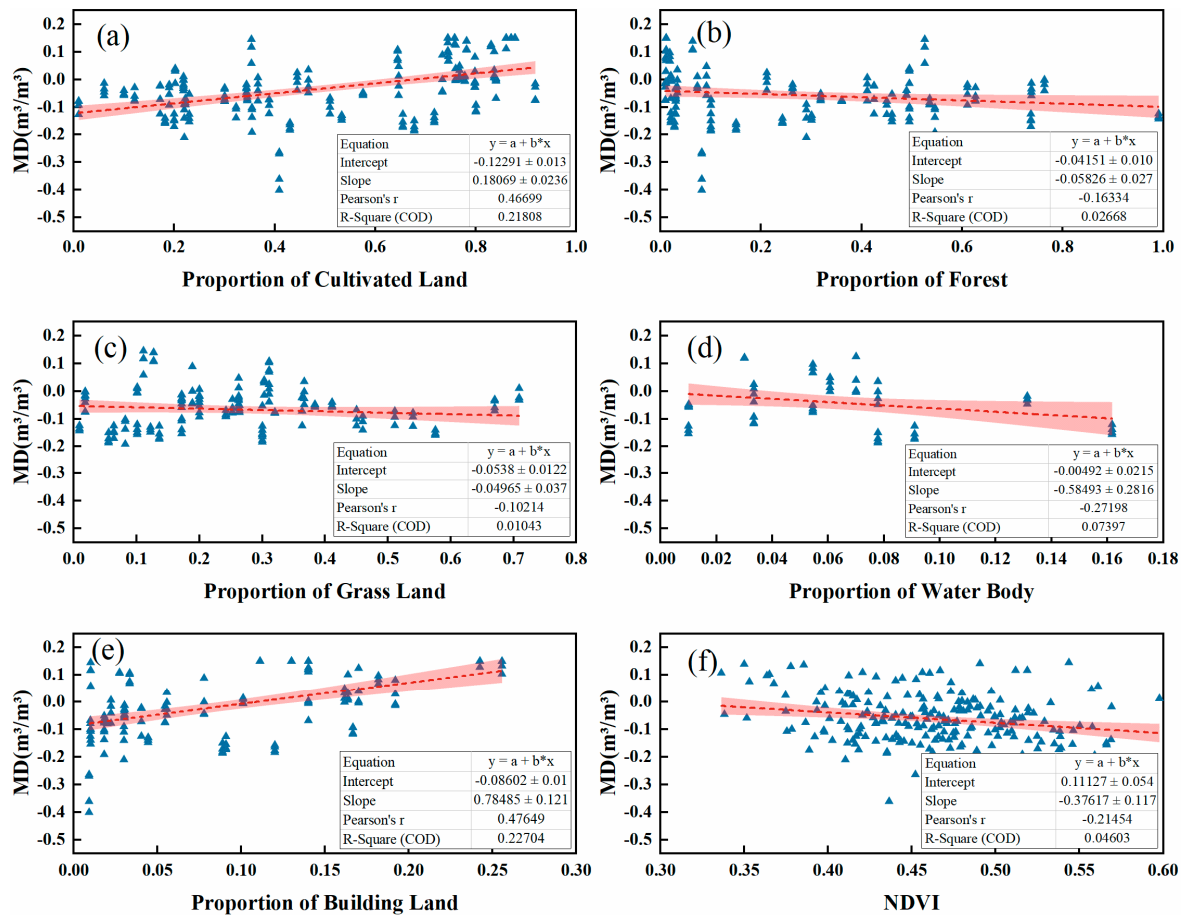


Figure 12. Scatter plots of the mean difference (MD) of SMAP soil moisture product relative to six environmental factors, with each plot excluding data points with an LUCC equal to 0: (a) Proportion of Cultivated Land; (b) Proportion of Forest; (c) Proportion of Grass Land; (d) Proportion of Water Body; (e) Proportion of Building Land; (f) NDVI.

The scatter plot excluded data points with a proportion of zero for any land use type to avoid any impact on the correlation. Satellite data included soil information and surface and subsurface water information. In this regard, a significant positive correlation is observed between the soil moisture content and electrical conductivity of cultivated land. However, for forest and grass land, the correlation between soil moisture content and electrical conductivity is not deemed significant [53]. In the study area, cultivated land primarily supports crops such as cotton, corn, and wheat, which have substantial water requirements throughout the year. Additionally, the electrical conductivity of water is considerably higher than that of soil. Satellite remote sensing demonstrates a heightened sensitivity to electrical conductivity [54]. Consequently, the soil moisture in the cultivated land is higher than the normal values, which leads to a positive correlation with the measured data (MD). Conversely, for building land, the electrical conductivity of concrete is lower than that of soil, and the soil moisture content is relatively low, resulting in the soil moisture of building land being lower than normal values and leading to a positive correlation with the measured data (MD). In the case of forest and grass land, the soil moisture and electrical conductivity do not exhibit a significant correlation, and the satellite

soil moisture product detects soil moisture within the normal range. Consequently, these areas show a negative correlation with the soil moisture data.

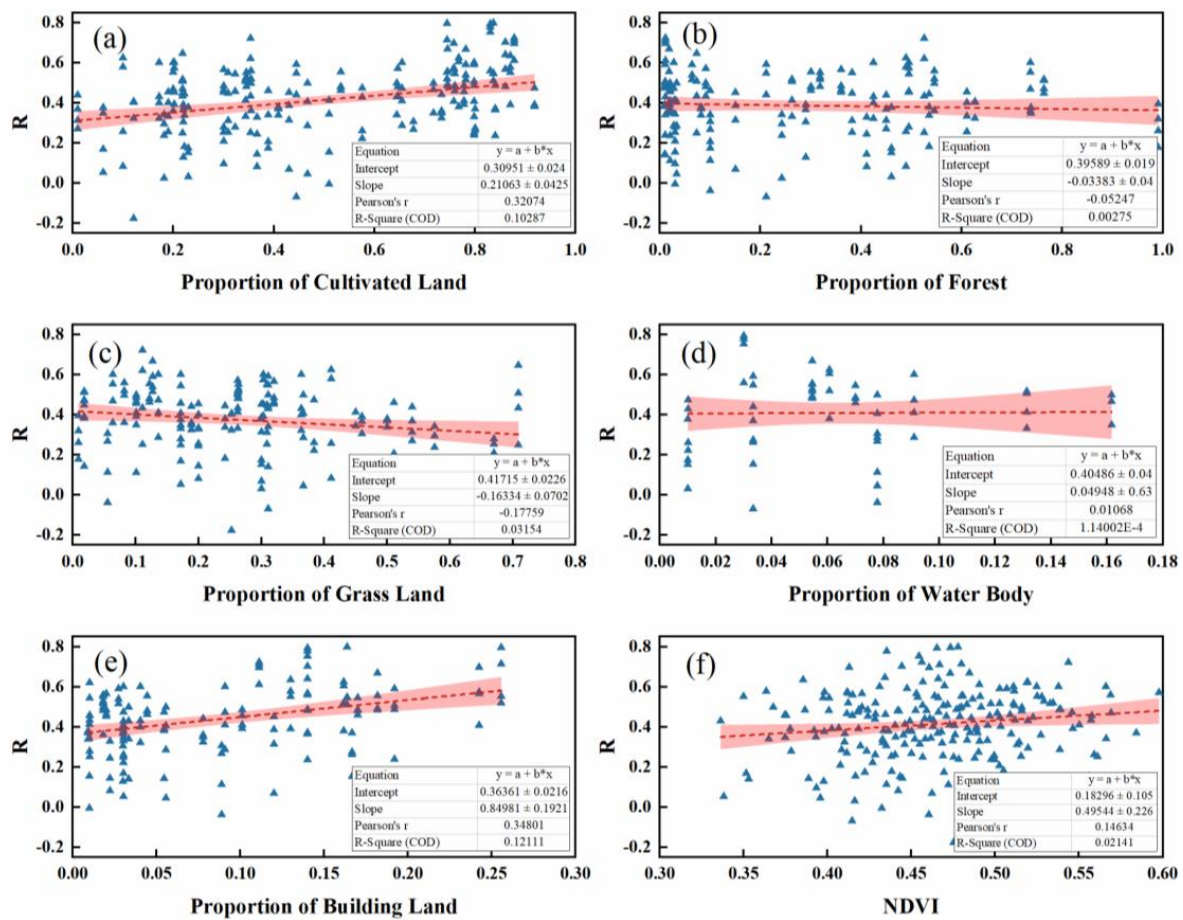


Figure 13. Scatter plots of the R of SMAP soil moisture product relative to six environmental factors, with each plot excluding data points with an LUCC equal to 0: (a) Proportion of Cultivated Land; (b) Proportion of Forest; (c) Proportion of Grass Land; (d) Proportion of Water Body; (e) Proportion of Building Land; (f) NDVI.

Figure 13 shows that R has a high positive correlation with cultivated land, water bodies, and building land. These regions were predominantly covered with low-lying crops, water bodies, or no vegetation, resulting in lower biomass characterized by flat terrain. Consequently, the soil moisture product was less affected by vegetation in these regions. This finding is consistent with the findings of Zeng et al. [55], who concluded that satellite soil moisture products yield better correlation results in areas with sparse vegetation. In contrast, the extensive vegetation coverage, tall and lush trees, and high biodiversity in forests and grasslands resulted in larger errors, leading to a negative correlation between R and these two land use types [56].

The negative correlation between NDVI and MD, as well as the positive correlation between NDVI and R, were in line with statistical logic. Nevertheless, a comprehensive exploration of the correlation between NDVI and statistical parameters, along with an in-depth examination of the underlying mechanisms, are required due to the myriad of factors influencing vegetation indices.

It is important to acknowledge that L-band satellite SM products are limited to providing near-surface soil moisture measurements at a depth of 5 cm. In this study, an assumption was made that the in situ soil moisture at 10 cm depth closely approximates that at 5 cm. Consequently, the in situ measurements at 10 cm were utilized as a reference to assess the performance of the SPL3SMP_E SM products. While this approach capitalizes on

the availability of dense soil moisture stations in the study area, it unavoidably introduces uncertainty into the evaluation process. Additionally, the spatial mismatch between the grid-based satellite observations and point-specific in situ measurements further complicates the interpretation of results. This disparity may explain why the statistical analysis indicates a larger bias in the SPL3SMP_E SM product compared to its intended design accuracy within this study. It underscores the need for careful consideration of depth assumptions and spatial discrepancies when evaluating satellite-derived soil moisture data.

6. Conclusions

This study employed measured soil moisture data from 55 soil moisture monitoring stations in Henan Province, along with precipitation data from meteorological stations, to validate the accuracy of the SPL3SMP_E soil moisture product. In addition, this study analyzed the response of the SPL3SMP_E soil moisture product to irrigation practices, and the study explored the performance of the SPL3SMP_E soil moisture product in drought monitoring. Firstly, this study calculated the differences in statistical indicators between the in situ soil moisture data and the SPL3SMP_E soil moisture data. Then, we conducted an analysis of the temporal and spatial variations in these statistical indicators and conducted significance tests to discern any notable differences. Subsequently, the correlation between accuracy indicators and environmental variables was calculated to gain an understanding of how various factors may influence the performance of the SPL3SMP_E soil moisture product. Next, the response of the satellite soil moisture product to irrigation signals based on the records of precipitation and irrigation at the monitoring stations was investigated. This specific aspect distinguished this research from other accuracy validation studies, as it focused on understanding how well the satellite product captures irrigation-related changes in soil moisture. Finally, this study utilized machine learning algorithms to apply the SPL3SMP_E soil moisture product for agricultural drought monitoring. Based on the results, the following conclusions were drawn: (1) The overall accuracy of the SPL3SMP_E soil moisture product was high, and the four statistical indicators (MD, RMSE, ubRMSE, and R) showed no significant differences over time but exhibit significant spatial clustering. (2) The accuracy of the SPL3SMP_E soil moisture product exhibited a significant correlation with land use types and vegetation indices. (3) The SPL3SMP_E soil moisture product performed well in capturing irrigation signals. (4) With the aid of the SPL3SMP_E soil moisture product and machine learning algorithms, it is possible to effectively monitor major drought events, while combining various indices can enhance the accuracy of drought monitoring.

Author Contributions: Conceptualization, L.Z. and M.D.; methodology, L.Z. and A.-X.Z.; software, H.W., G.T. and T.M.; validation, L.Z. and T.M.; formal analysis, L.Z., M.D.; investigation, L.Z.; resources, L.Z.; data curation, L.Z. and G.T.; writing—original draft preparation, L.Z. and G.T.; writing—review and editing, L.Z.; visualization, L.Z. and M.D.; supervision, L.Z.; project administration, L.Z. All authors have read and agreed to the published version of the manuscript.

Funding: This research was funded by the Natural Science Foundation of Jiangsu Province (No. BK20230603), the Foundation of Anhui Province Key Laboratory of Physical Geographic Environment, P.R. China (No. 2022PGE002), Postdoctoral Research Funding Program of Jiangsu Province (No. 2020Z223), and the Natural Science Foundation of Anhui Province (No. 2208085QD108).

Data Availability Statement: The raw data supporting the conclusions of this article will be made available by the authors on request.

Conflicts of Interest: The authors declare no conflicts of interest.

References

1. Ochsner, E.T.; Cosh, H.M.; Cuenca, H.R.; Cuenca, W.A.; Dorigo, C.S.; Draper, Y.H.; Yann, H.; Kerr, K.M.; Larson, E.G. State of the Art in Large-Scale Soil Moisture Monitoring. *Soil Sci. Soc. Am. J.* **2013**, *77*, 6–8. [[CrossRef](#)]
2. Mason, P.J.; Zillman, J.W.; Simmons, A. Implementation plan for the global observing system for climate in support of the UNFCCC. In Proceedings of the Conference of the Parties (COP), Copenhagen, Denmark, 7–18 December 2009.

3. Li, Y.; Liu, D.; Li, T.; Fu, Q.; Liu, D.; Hou, R.J.; Meng, F.Q.; Li, M.; Li, Q.L. Responses of spring soil moisture of different land use types to snow cover in Northeast China under climate change background. *J. Hydrol.* **2022**, *608*, 127610. [[CrossRef](#)]
4. Cao, M.; Chen, M.; Liu, J.; Liu, Y.L. Assessing the performance of satellite soil moisture on agricultural drought monitoring in the North China Plain. *Agric. Water Manag.* **2022**, *263*, 107450. [[CrossRef](#)]
5. Vincent, H.; Alexis, B.; Philippe, C.; Gentine, P.; Jung, M.; Reichstein, M.; Seneviratne, S.I.; Frankenberg, C. Soil moisture–atmosphere feedback dominates land carbon uptake variability. *Nature* **2021**, *592*, 7852.
6. Chen, P.; Duan, Y.; Liang, J. Soil Moisture Extraction Based on Time-Frequency Analysis. In Proceedings of the International Conference in Communications, Seoul, Republic of Korea, 16–20 May 2022; Springer Nature Singapore: Singapore, 2022.
7. Abowarda, A.S.; Bai, L.; Zhang, C.; Long, D.; Li, X.; Huang, Q.; Sun, Z. Generating surface soil moisture at 30 m spatial resolution using both data fusion and machine learning toward better water resources management at the field scale. *Remote Sens. Environ.* **2021**, *555*, 112301. [[CrossRef](#)]
8. Luo, S. *Dedicated Satellite Remote Sensing Combined with Global Navigation Satellite System Data Used to Remotely Measure the Status of Land Desertification*; Yan'an University, School of Physics and Electronics Information: Yan'an, China, 2022.
9. Ma, Y.; Zhu, W.; Zhang, Z.; Chen, H.; Zhao, G.; Liu, P. Fusion level of satellite and UAV image data for soil salinity inversion in the coastal area of the Yellow River Delta. *Int. J. Remote Sens.* **2022**, *43*, 7039–7063. [[CrossRef](#)]
10. Li, Z.; Chen, J.; Liu, Y. Soil moisture retrieval from remote sensing. *J. Beijing Norm. Univ.* **2020**, *56*, 474–481.
11. Qin, X.D.; Pang, Z.G.; Jiang, W.; Feng, T.; Fu, J. Progress and development trend of soil moisture microwave remote sensing retrieval method. *J. Geo-Inf. Sci.* **2021**, *23*, 1728–1742.
12. Colliander, A.; Reichle, R.H.; Crow, W.T.; Chen, F.; Chan, S.V.; Das, N.N.; Bindlish, R.; Chaubell, J.; Kim, S. Validation of soil moisture data products from the NASA SMAP mission. *IEEE J. Sel. Top. Appl. Earth Obs. Remote Sens.* **2021**, *15*, 364–392. [[CrossRef](#)]
13. Kerr, Y.; Al-Yaari, A.; Rodriguez-Fernandez, N.; Parrons, M.; Molero, B.; Leroux, D.; Bircher, S.; Mahmoodi, A.; Mialon, A.; Richaume, P.; et al. Overview of SMOS performance in terms of global soil moisture monitoring after six years in operation. *Remote Sens. Environ.* **2016**, *180*, 40–63. [[CrossRef](#)]
14. Entekhabi, D.; Njoku, G.E.; O'Neill, P.; Kellogg, K.H.; Crow, W.T.; Edelstein, W.N.; Entin, J.K.; Goodman, S.D.; Jackson, T.J.; Johnson, J. The Soil Moisture Active Passive (SMAP) Mission. *Proc. IEEE* **2010**, *98*, 704–716. [[CrossRef](#)]
15. Figa-Saldaña, J.; Wilson, J.J.; Attema, E.; Gelsthorpe, R.; Drinkwater, M.R.; Stoffelen, A. The advanced scatterometer (ASCAT) on the meteorological operational (MetOp) platform: A follow on for European wind scatterometers. *Int. J. Remote Sens.* **2002**, *28*, 404–412. [[CrossRef](#)]
16. Derin, Y.; Anagnostou, E.; Anagnostou, M.N.; Kalogiros, J.; Casella, D.; Marra, A.C.; Panegrossi, G.; Sanò, P. Passive Microwave Rainfall Error Analysis Using High-Resolution X-Band Dual-Polarization Radar Observations in Complex Terrain. *IEEE Trans. Geosci. Remote Sens.* **2018**, *56*, 2565–2586. [[CrossRef](#)]
17. Liu, X.G.; Hui, H.Z. Experimental Study of C Band Passive Microwave Remote Sensing of Soil Moisture. *Appl. Mech. Mater* **2013**, *13*, 477–478.
18. Ye, N.; Walker, J.P.; Yeo, I.Y.; Jackson, T.J.; Kerr, Y.; Kim, E.; Mcgrath, A.; Popstefanija, I.; Goodberlet, M.; Hills, J. Toward P-Band Passive Microwave Sensing of Soil Moisture. *IEEE Geosci. Remote Sens. Lett.* **2020**, *18*, 504–508. [[CrossRef](#)]
19. Wigneron, J.P.; Li, X.J.; Frappart, F.; Fan, L.; Al-Yaari, A.; De Lannoy, G.; Liu, X.; Wang, M.; Le Masson, E.; Moisy, C. SMOS-IC data record of soil moisture and L-VOD: Historical development, applications and perspectives. *Remote Sens. Environ.* **2021**, *254*, 112238. [[CrossRef](#)]
20. Ma, H.; Li, X.; Zeng, J.; Zhang, X.; Dong, J.; Chen, N.; Fan, L.; Sadeghi, M.; Frappart, F.; Liu, X. An assessment of L-band surface soil moisture products from SMOS and SMAP in the tropical areas. *Remote Sens. Environ.* **2023**, *284*, 113344. [[CrossRef](#)]
21. Tian, S.; Renzullo, L.J.; Pipunic, R.C.; Lerat, J.; Sharples, W.; Donnelly, C. Satellite soil moisture data assimilation for improved operational continental water balance prediction. *Hydrol. Earth Syst. Sci.* **2021**, *25*, 4567–4584. [[CrossRef](#)]
22. Wen, Y.; Zhao, J.; Zhu, G.; Xu, R.; Yang, J. Evaluation of the RF-Based Downscaled SMAP and SMOS Products Using Multi-Source Data over an Alpine Mountains Basin, Northwest China. *Water* **2021**, *13*, 2875. [[CrossRef](#)]
23. Fernandez-Moran, R.; Al-Yaari, A.; Mialon, A.; Mahmoodi, A.; Al Bitar, A.; De Lannoy, G.; Rodriguez-Fernandez, N.; Lopez-Baeza, E.; Kerr, Y.; Wigneron, J.P. SMOS-IC: An Alternative SMOS Soil Moisture and Vegetation Optical Depth Product. *Remote Sens* **2017**, *9*, 457. [[CrossRef](#)]
24. Chan, K.S.; Bindlish, R.; O'Neill, E.P.; Njoku, E.; Jackson, T.; Colliander, A.; Chen, F.; Burgin, M.; Dunbar, S.; Piepmeier, J. Assessment of the SMAP Passive Soil Moisture Product. *IEEE Trans. Geosci. Remote Sens.* **2016**, *54*, 4994–5007. [[CrossRef](#)]
25. Zhang, P.; Yu, H.; Gao, Y.; Zhang, Q. Evaluation of Remote Sensing and Reanalysis Products for Global Soil Moisture Characteristics. *Sustainability* **2023**, *15*, 9112. [[CrossRef](#)]
26. Zhu, L.; Liu, J.; Zhu, A.X.; Duan, Z. Spatial evaluation of L-band satellite-based soil moisture products in the upper Huai River basin of China. *Eur. J. Remote Sens.* **2019**, *52*, 194–205. [[CrossRef](#)]
27. Kim, S.; Dong, J.; Sharma, A. A triple collocation-based comparison of three L-band soil moisture datasets, SMAP, SMOS-IC, and SMOS, over varied climates and land covers. *Front. Environ. Sci.* **2021**, *3*, 693172. [[CrossRef](#)]
28. Li, C.; Lu, H.; Yang, K.; Han, M.; Wright, J.S.; Chen, Y.; Yu, L.; Xu, S.; Huang, X.; Gong, W. The Evaluation of SMAP Enhanced Soil Moisture Products Using High-Resolution Model Simulations and In-Situ Observations on the Tibetan Plateau. *Remote Sens.* **2018**, *10*, 535. [[CrossRef](#)]

29. Lawston, M.P.; Santanello, A.J.; Kumar, V.S. Irrigation Signals Detected From SMAP Soil Moisture Retrievals. *Geophys. Res. Lett.* **2017**, *44*, 11.860–11.867. [[CrossRef](#)]
30. Zhu, L.; Zhu, A.X. Extraction of Irrigation Signals by Using SMAP Soil Moisture Data. *Remote Sens.* **2021**, *13*, 2142. [[CrossRef](#)]
31. Dar, I.; Qadir, J.; Shukla, A. Estimation of LST from Multi-Sensor Thermal Remote Sensing Data and Evaluating the Influence of Sensor Characteristics. *Ann. GIS* **2019**, *25*, 263–281. [[CrossRef](#)]
32. Dari, J.; Brocca, L.; Quintana-Seguí, P.; Casadei, S.; Escorihuela, M.J.; Stefan, V.; Morbidelli, R. Double-scale analysis on the detectability of irrigation signals from remote sensing soil moisture over an area with complex topography in central Italy. *Adv. Water Resour.* **2022**, *161*, 104130. [[CrossRef](#)]
33. Gómez, D.G.; Ochoa, C.G.; Godwin, D.; Tomasek, A.A.; Re, M.I.Z. Soil Moisture and Water Transport through the Vadose Zone and into the Shallow Aquifer: Field Observations in Irrigated and Non-Irrigated Pasture Fields. *Land* **2022**, *11*, 2029. [[CrossRef](#)]
34. Pascal, C.; Ferrant, S.; Rodriguez-Fernandez, N.; Kerr, Y.; Selles, A.; Merlin, O. Indicator of flood-irrigated crops from SMOS and SMAP soil moisture products in southern India. *IEEE Geosci.* **2023**, *20*, 4500205. [[CrossRef](#)]
35. Mladenova, E.I.; Bolten, D.J.; Crow, W.; Crow, W.; Sazib, N.; Reynolds, C. Agricultural Drought Monitoring via the Assimilation of SMAP Soil Moisture Retrievals into a Global Soil Water Balance Model. *Front. Big Data* **2020**, *3*, 10. [[CrossRef](#)] [[PubMed](#)]
36. Peng, J.; Niesel, J.; Loew, A.; Zhang, S.; Wang, J. Evaluation of Satellite and Reanalysis Soil Moisture Products over Southwest China Using Ground-Based Measurements. *Remote Sens.* **2015**, *7*, 15729–15747. [[CrossRef](#)]
37. Lorenz, C.; Montzka, C.; Jagdhuber, T.; Laux, P.; Kunstmann, H. Long-Term and High-Resolution Global Time Series of Brightness Temperature from Copula-Based Fusion of SMAP Enhanced and SMOS Data. *Remote Sens.* **2018**, *10*, 1842. [[CrossRef](#)]
38. O'Neill, P.; Chan, S.; Colliander, A.; Dunbar, S.; Njoku, E.; Bindlish, R.; Chen, F.; Jackson, T.; Burgin, M.; Piepmeier, J.; et al. Evaluation of the validated Soil Moisture product from the SMAP radiometer. In Proceedings of the 2016 IEEE International Geoscience and Remote Sensing Symposium (IGARSS), Beijing, China, 10–15 July 2016; pp. 125–128.
39. O'Neill, P.; Chan, E. *SMAP Enhanced L3 Radiometer Global Daily 9 km EASE-Grid Soil Moisture*; NASA/SMAP/SPL3SMP_E/005; NASA National Snow and Ice Data Center Distributed Active Archive Center: Boulder, CO, USA, 2019.
40. Deng, K.; Petropoulos, G.P.; Bao, Y.; Pavlides, A.; Chaibou, A.S.; Habtemicheal, B.A. An Examination of the SMAP Operational Soil Moisture Products Accuracy at the Tibetan Plateau. *Remote Sens.* **2022**, *24*, 6255. [[CrossRef](#)]
41. Khare, S.; Latifi, H.; Khare, S. Vegetation Growth Analysis of UNESCO World Heritage Hyrcanian Forests Using Multi-Sensor Optical Remote Sensing Data. *Remote Sens.* **2021**, *13*, 3965. [[CrossRef](#)]
42. Entekhabi, D.; Reichle, R.H.; Koster, R.D.; Crow, W.T. Performance metrics for soil moisture retrievals and application requirements. *J. Hydrometeorol.* **2010**, *11*, 832–840. [[CrossRef](#)]
43. Wang, Z.; Che, T.; Zhao, T.; Crow, W.T. Evaluation of SMAP, SMOS, and AMSR2 soil moisture products based on distributed ground observation network in cold and arid regions of China. *IEEE J. Sel. Top. Appl. Earth Obs. Remote Sens.* **2021**, *14*, 8955–8970. [[CrossRef](#)]
44. Kumar, S.V.; Peters-Lidard, C.D.; Santanello, J.A.; Reichle, R.H.; Draper, C.S.; Koster, R.D.; Nearing, G.; Jasinski, M.F. Evaluating the utility of satellite soil moisture retrievals over irrigated areas and the ability of land data assimilation methods to correct for unmodeled processes. *Hydrol. Earth Syst. Sci.* **2015**, *19*, 4463–4478. [[CrossRef](#)]
45. Zhang, K.; Li, X.; Zheng, D.; Zhang, L.; Zhu, G. Estimation of Global Irrigation Water Use by the Integration of Multiple Satellite Observations. *Water Resour. Res.* **2022**, *58*, e2021WR030031. [[CrossRef](#)]
46. Li, X.; Xin, X.; Jiao, J.; Peng, Z.; Zhang, H.; Shao, S.; Liu, Q. Estimating Subpixel Surface Heat Fluxes through Applying Temperature-Sharpener Methods to MODIS Data. *Remote Sens.* **2017**, *9*, 836. [[CrossRef](#)]
47. Li, X.; Wigneron, J.P.; Frappart, F.; De Lannoy, G.; Fan, L.; Zhao, T.J.; Gao, L.; Tao, S.L.; Ma, H.L.; Peng, Z.Q. The first global soil moisture and vegetation optical depth product retrieved from fused SMOS and SMAP L-band observations. *Remote Sens. Environ.* **2022**, *282*, 113272. [[CrossRef](#)]
48. Kim, H.; Parinussa, R.; Konings, A.; Wagner, W.; Cosh, M.; Lakshmi, V.; Zohaib, M.; Choi, M. Global-scale assessment and combination of SMAP with ASCAT (active) and AMSR2 (passive) soil moisture products. *Remote Sens. Environ.* **2018**, *204*, 260–275. [[CrossRef](#)]
49. Nadeem, A.A.; Zha, Y.; Shi, L.; Ran, G.; Ali, S.; Jahangir, Z.; Afzal, M.; Awais, M. Multi-Scale Assessment of SMAP Level 3 and Level 4 Soil Moisture Products over the Soil Moisture Network within the ShanDian River (SMN-SDR) Basin, China. *Remote Sens.* **2022**, *14*, 982. [[CrossRef](#)]
50. Colliander, A.; Jackson, J.T.; Berg, A.; Bosch, D.D.; Caldwell, T.; Chan, S.; Cosh, M.H.; Collins, C.H.; Martínez-Fernández, J.; McNairn, H. Effect of Rainfall Events on SMAP Radiometer-Based Soil Moisture Accuracy Using Core Validation Sites. *J. Hydrometeorol.* **2020**, *21*, 255–264. [[CrossRef](#)]
51. Gemechu, M.G.; Hulluka, T.A.; Wakjira, Y.C. Analysis of Spatiotemporal Variability of Water Productivity in Ethiopian Sugar Estates: Using Open Access Remote Sensing Source. *Ann. GIS* **2020**, *26*, 395–405. [[CrossRef](#)]
52. Sawadogo, A.; Kouadio, L.; Traoré, F.; Zwart, S.J.; Hessels, T.; Gündogdu, K.S. Spatiotemporal Assessment of Irrigation Performance of the Kou Valley Irrigation Scheme in Burkina Faso Using Satellite Remote Sensing-Derived Indicators. *ISPRS Int. J. Geoinf.* **2020**, *9*, 484. [[CrossRef](#)]
53. Price, K.; Jackson, R.C.; Parker, J.A. Variation of surficial soil hydraulic properties across land uses in the southern Blue Ridge Mountains, North Carolina, USA. *J. Hydrol.* **2009**, *383*, 256–268. [[CrossRef](#)]

54. Masayasu, M.; Supranee, S.; Mallika, S.; Koshi, Y.; Koki, H.; Somsak, S. Impact of changes in the relationship between salinity and soil moisture on remote sensing data usage in northeast Thailand. *Hydrol. Res. Lett.* **2022**, *16*, 54–58.
55. Zeng, J.; Li, Z.; Chen, Q.; Bi, H.; Qiu, J.; Zou, P. Evaluation of remotely sensed and reanalysis soil moisture products over the Tibetan Plateau using in-situ observations. *Remote Sens. Environ.* **2015**, *163*, 91–110. [[CrossRef](#)]
56. Sun, Y.; Huang, S.; Ma, J.; Li, J.; Li, X.; Wang, H.; Chen, S.; Zang, W. Preliminary Evaluation of the SMAP Radiometer Soil Moisture Product over China Using In Situ Data. *Remote Sens.* **2017**, *9*, 292. [[CrossRef](#)]

Disclaimer/Publisher’s Note: The statements, opinions and data contained in all publications are solely those of the individual author(s) and contributor(s) and not of MDPI and/or the editor(s). MDPI and/or the editor(s) disclaim responsibility for any injury to people or property resulting from any ideas, methods, instructions or products referred to in the content.